Estimation of Consistent Global Microwave Land Surface Emissivity from AMSR-E and AMSR2 Observations

SATYA PRAKASH AND HAMID NOROUZI[a]

New York City College of Technology, City University of New York, Brooklyn, New York

MARZI AZARDERAKHSH

School of Computer Science and Engineering, Fairleigh Dickinson University, Teaneck, New Jersey

REGINALD BLAKE

New York City College of Technology, City University of New York, Brooklyn, New York

CATHERINE PRIGENT

Laboratoire d'Études du Rayonnement et de la Matière en Astrophysique et Atmosphères, CNRS, Observatoire de Paris, Paris, France

REZA KHANBILVARDI

NOAA Center for Earth System Sciences and Remote Sensing Technologies, and City College of the City University of New York, New York, New York

(Manuscript received 29 July 2017, in final form 28 November 2017)

ABSTRACT

Accurate estimation of passive microwave land surface emissivity (LSE) is crucial for numerical weather prediction model data assimilation, for microwave retrievals of land precipitation and atmospheric profiles, and for a better understanding of land surface and subsurface characteristics. In this study, global instantaneous LSE is estimated for a 9-yr period from the Advanced Microwave Scanning Radiometer for Earth Observing System (AMSR-E) and for a 5-yr period from the Advanced Microwave Scanning Radiometer 2 (AMSR2) sensors. Estimates of LSE from both sensors were obtained by using an updated algorithm that minimizes the discrepancy between the differences in penetration depths from microwave and infrared remote sensing observations. Concurrent ancillary datasets such as skin temperature from the Moderate Resolution Imaging Spectroradiometer (MODIS) and profiles of air temperature and humidity from the Atmospheric Infrared Sounder are used. The latest collection 6 of MODIS skin temperature is used for the LSE estimation, and the differences between collections 6 and 5 are also comprehensively assessed. Analyses reveal that the differences between these two versions of infrared-based skin temperatures could lead to approximately a 0.015 difference in passive microwave LSE values, especially in arid regions. The comparison of global mean LSE features from the combined use of AMSR-E and AMSR2 with an independent product—Tool to Estimate Land Surface Emissivity from Microwave to Submillimeter Waves (TELSEM^2)—shows spatial pattern correlations of order 0.92 at all frequencies. However, there are considerable differences in magnitude between these two LSE estimates, possibly because of differences in incidence angles, frequencies, observation times, and ancillary datasets.

1. Introduction

Reliable instantaneous estimates of land surface emissivity (LSE) are vital for the accurate retrieval of atmospheric variables, for the study of vegetation phenology, for the understanding of land surface and subsurface processes, and for the application of data

[a] Additional affiliation: Earth and Environmental Sciences, the Graduate Center, City University of New York, New York, New York.

Corresponding author: Hamid Norouzi, hnorouzi@citytech.cuny.edu

DOI: 10.1175/JAMC-D-17-0213.1

assimilation techniques in numerical weather prediction models (Prigent et al. 1998; Matzler 2005; Aires et al. 2011; Gerard et al. 2011; Ferraro et al. 2013; Turk et al. 2014; Prakash et al. 2017). Unlike over the ocean, microwave emissivity over land is highly variable because of a plethora of surface characteristics that include soil moisture, soil texture, surface roughness, land-cover type, and vegetation optical depth.

During the last three decades, substantial progress has been made in retrieving LSE from passive microwave (PMW) sensors. Retrieval algorithms are broadly based on land surface models and direct satellite observations (Ferraro et al. 2013; Turk et al. 2014; Ringerud et al. 2015; Tian et al. 2015). To model the interaction of electromagnetic waves with surface components, land surface model–based retrievals require a large number of surface parameters that are not easily available or observable at the global scale. Direct observational-based algorithms use satellite brightness temperature (Tb) observations along with corresponding land and atmospheric properties to retrieve LSE. This type of retrieval algorithm is supposed to be computationally easier and more reliable than the land surface model–based retrievals. Most of the PMW satellite retrievals, such as Special Sensor Microwave Imager (SSM/I; Prigent et al. 2006), Advanced Microwave Scanning Radiometer for Earth Observing System (AMSR-E; Norouzi et al. 2011), Advanced Microwave Scanning Radiometer 2 (AMSR2; Prakash et al. 2016), Advanced Microwave Sounding Unit (AMSU; Karbou et al. 2005), and Microwave Analysis and Detection of Rain and Atmospheric Structures (MADRAS; Raju et al. 2013), use this approach for LSE retrieval at the global scale. These retrievals generally use simultaneous infrared-based land surface temperature (LST, or skin temperature) and profiles of air temperature and humidity to estimate LSE. Estimates of LSE from these PMW sensors were derived by minimizing atmospheric effects from Tbs and by the efficient characterization of land surface geophysical states. However, because of the dependence on infrared-based ancillary data, this type of retrieval provides LSE estimates only for cloud-free regions.

Passive microwave LSE estimates have recently been utilized for various applications such as snowpack detection (Shahroudi and Rossow 2014), detection and estimation of land precipitation (Birman et al. 2015), and detection of soil freezing and thawing (Prakash et al. 2017). However, a comprehensive assessment of uncertainty in these LSE estimates, based on distinct algorithms and input datasets, is essential for their wider applicability. The validation of LSE estimates at the global scale is challenging because of the paucity of ground-based observations. Moreover, few studies have been conducted to validate these LSE estimates at selected ground stations or to intercompare different satellite-based LSE products at the global scale (Tian et al. 2014; Norouzi et al. 2015a; Prigent et al. 2015). Although LSE estimates from different algorithms and sensors reproduce similar large-scale features and seasonal variability, they notably differ from one another at the monthly time scale. These discrepancies are primarily due to differences in the configuration of sensors—for example, frequency, polarization, incident angle, footprint, and overpass time—as well as the relative differences in retrieval methods and ancillary datasets. Moreover, most LSE estimates utilize reanalysis products as ancillary inputs that generally need to be interpolated. Therefore, the use of a common algorithm and ancillary data for multiple satellite observations would essentially reduce the uncertainty due to spatiotemporal interpolation and provide comprehensive maps of the global LSE estimates for a longer time period (Norouzi et al. 2015a).

Another source of uncertainty in the PMW-based LSE estimates at the global scale is the direct use of infrared-based LST, which does not essentially show diurnal characteristics similar to the PMW-based Tbs. Infrared-based LST has almost no penetration depth, whereas PMW-based Tbs have a distinct penetration depth depending on operating frequencies and vegetation types. Larger differences were noticed over regions with soil texture favorable for deeper penetration, for example, generally over the arid regions with sand dunes, by the PMW-based Tbs (Prigent et al. 1999; Norouzi et al. 2012, 2015b). Hence, the inconsistency between both parameters should be vigilantly addressed in order to improve the estimation of reliable LSEs. Norouzi et al. (2012) proposed an efficient method to alleviate such a discrepancy. After some simplifications, this method was recently used to retrieve LSEs from the AMSR2 sensor (Prakash et al. 2016). Furthermore, since it is the norm for satellite products to undergo intermittent retrospective processing when updated, more accurate versions of products are released, it is reasonable to update the LSE estimates with the latest versions of input datasets for wider applicability.

The objective of this study is to develop a coherent instantaneous LSE estimate at the global scale by using the AMSR-E and AMSR2 sensors. These sensors have similar sensor characteristics and overpass times. The latest versions of PMW-based Tbs and concurrent infrared-based ancillary datasets are used for the retrieval of cloud-free LSE. The consistency of the estimated LSE from these two sensors is also investigated for different land-cover types.

2. Data and methods

a. AMSR-E and AMSR2 data

The *Aqua* and the *Global Change Observation Mission–Water* (*GCOM-W1*) satellites are the members of the afternoon constellation or A-Train, whose equatorial crossing times are about 1330/0130 local time. The *Aqua* satellite was launched on 4 May 2002 by the National Aeronautics and Space Administration (NASA), and among the sensors it carries are the AMSR-E, the Atmospheric Infrared Sounder (AIRS), and the Moderate Resolution Imaging Spectroradiometer (MODIS). The overall goal of the *Aqua* satellite and its suite of sensors is to study water in the Earth–atmosphere–biosphere system. However, AMSR-E stopped producing data in October 2011. On 18 May 2012, the Japan Aerospace Exploration Agency (JAXA) launched the *GCOM-W1* satellite. The satellite had the AMSR2 instrument onboard with the aim of studying changes in water circulation. AMSR-E was a six-frequency dual-polarized PMW radiometer that measured Tbs at 6.925, 10.65, 18.7, 23.8, 36.5, and 89.0 GHz (Kawanishi et al. 2003). AMSR2 has sensor characteristics similar to those of its predecessor AMSR-E, but it also included improvements such as an additional 7.3-GHz channel for radiofrequency interference mitigation and also improved calibration (Okuyama and Imaoka 2015). Like AMSR-E, AMSR2 has a conical scan mechanism, and it obtains data over a ~1450-km swath with a 55° incidence angle. In this study, level 3 global swath spatially resampled Tbs at 0.25° spatial resolution for all the frequency channels of AMSR-E (version 7) from October 2002 to September 2011 and AMSR2 (version 2.2) from July 2012 to June 2017 were used. These datasets were obtained from the GCOM-W research product distribution service at the JAXA.

b. Ancillary satellite data

To mitigate the atmospheric effects from the PMW measurements of Tbs, near-simultaneous infrared-based LST and profiles of air temperature and humidity were used. The latest collection of the MODIS version 6 (V6) cloud-free land surface temperature daily L3 swath global product (e.g., MYD11C1; Wan 2014) available at a 0.05° climate modeling grid (~5.6 km at the equator) were used. Large-scale changes in V6 of the global LST product relative to its predecessor V5 were also assessed. The daily level 3 globally gridded integrated water vapor and air temperature profiles from the AIRS infrared-only V6 (e.g., AIRS3STD; Susskind et al. 2014) available at 1° spatial resolutions were used. It is to be noted that version 6 of ancillary data from both MODIS and AIRS sensors, mounted on the sun-synchronous *Aqua* satellite, under clear-sky conditions were used. Thus, the estimated LSE would effectively benefit from the concurrence of satellite observations.

To compare mean features of the estimated LSE, the Tool to Estimate Land Surface Emissivity from Microwave to Submillimeter Waves (TELSEM^2) climatology was used. TELSEM^2 was developed to provide a reliable parameterization of LSE for frequencies up to 700 GHz for advancing data assimilation of radiances in numerical weather prediction models (Wang et al. 2017). The emissivity parameterization between 19 and 85 GHz is anchored to a monthly mean climatology of LSE computed from the SSM/I observations between 1993 and 2000 at a 0.25° equal-area grid.

c. Method for LSE estimation

Since the spatial resolutions of PMW-based Tbs and infrared-based ancillary data are different, all these orbital data were reprojected to a common equal-area grid (0.25° at the equator). The instantaneous global cloud-free land surface emissivity ε from AMSR-E and AMSR2 Tbs at polarization p and frequency ν conditions is computed using the following expression (Prigent et al. 2006):

$$\varepsilon_{(p,\nu)} = \frac{\mathrm{Tb}_{(p,\nu)} - T\uparrow - T\downarrow e^{-\tau(0,H)/\mu}}{e^{-\tau(0,H)/\mu}(T_s - T\downarrow)}, \tag{1}$$

where $T\uparrow$ and $T\downarrow$ are the upward and downward contribution of Tbs from the atmosphere at the surface, respectively, and they depend on incidence angle, atmospheric absorption, and extinction. The atmospheric temperature and humidity play a key role in the determination of these parameters through a suitable microwave radiative transfer model (Norouzi et al. 2011). The term T_s stands for skin temperature or LST, μ is the cosine of the incidence angle, and τ denotes the atmospheric opacity between two altitudes. The estimated cloud-free land emissivity using Eq. (1) may produce inconsistent LSE values between day and night by up to 12% because of the use of infrared-based LST instead of effective temperature at the depth of PMW observations. There exists a considerable difference in the diurnal cycle amplitude and phase between PMW-based Tbs and infrared-based LST, primarily in arid regions, where moisture and vegetation are scarce and cover about 45% of the global land areas (Norouzi et al. 2012, 2015b). To minimize this difference and produce more accurate LSE estimates, a statistical correction factor is applied to the MODIS LST over arid regions. The correction factor for the MODIS LST is computed for each month based on the

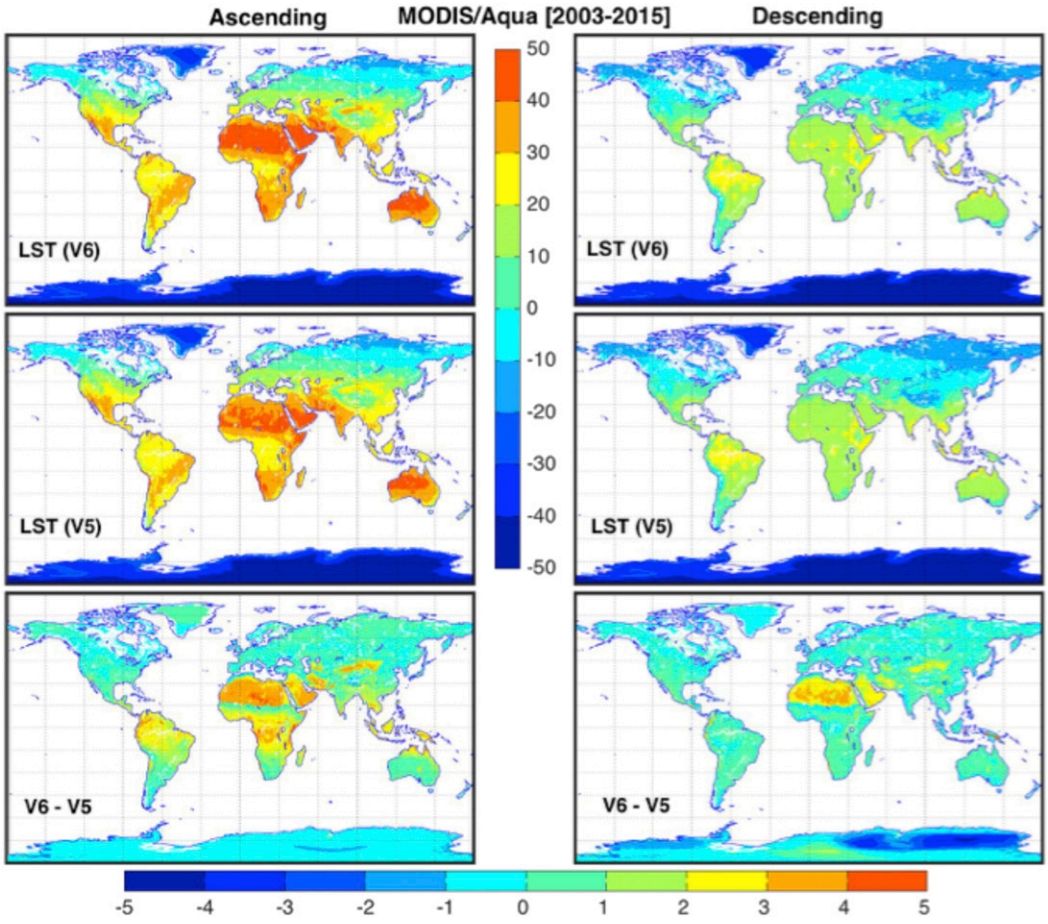

FIG. 1. Spatial distributions of mean global LSTs (°C) from MODIS *Aqua* V6 and V5 products for day (ascending) and night (descending) overpasses and their differences averaged for the period from January 2003 to December 2015.

mean passive microwave Tbs for day and night overpasses based on the following equation:

$$T^{C}_{s(t)} = T_{s(t)} \pm \frac{\overline{\mathrm{Tb}_{\mathrm{day}(t)}} - \overline{\mathrm{Tb}_{\mathrm{night}(t)}}}{2}, \qquad (2)$$

where $\overline{\mathrm{Tb}_{\mathrm{day}(t)}}$ and $\overline{\mathrm{Tb}_{\mathrm{night}(t)}}$ are the mean composite Tbs for all the day and night overpasses for a specific month, respectively, $T^{C}_{s(t)}$ is the corrected effective temperature consistent with PMW data, and $T_{s(t)}$ is the mean daily skin temperature. A detailed description of this statistical method is provided by Prakash et al. (2016). However, this statistical method is suitable for the estimation of instantaneous cloud-free LSE. Hence, the LSE estimates presented in this study use an improved algorithm and common observational input datasets. The errors in LSE retrieval due to the uncertainties in ancillary atmospheric datasets were explicitly quantified by Norouzi et al. (2011). Thus, the use of concurrent ancillary datasets would essentially reduce the uncertainty in the LSE estimates.

3. Results and discussion

a. *Comparison between* Aqua *MODIS V5 and V6 LST products*

Since mid-2002, the MODIS sensor on board the *Aqua* satellite has used a split-window algorithm to provide LST products. The MODIS-derived LST products have been effectively used to retrieve near-surface air temperature at the regional scale. These retrieved near-surface air temperatures are vital for a wide range of applications in agriculture, hydrology, surface energy budget analysis, and meteorology (Noi et al. 2016; Didari et al. 2017). In this section, V6 and V5 of the *Aqua* MODIS LST products are intercompared for the period of 2003–15. Figure 1 shows the spatial distributions of mean daytime (ascending orbits) and nighttime (descending orbits) LST from V6 and V5 products and their corresponding differences. The broadscale mean features such as higher LST over the arid regions and

TABLE 1. Mean MODIS *Aqua* LST (°C) averaged over the period from January 2003 to December 2015.

	Ascending		Descending	
	V6	V5	V6	V5
Globe (90°S–90°N)	17.20	16.20	2.19	2.00
Northern Hemisphere (0°–90°N)	19.78	18.76	3.80	3.33
Southern Hemisphere (0°–90°S)	12.67	11.67	−0.83	−0.55
Tropics (30°S–30°N)	33.03	31.14	15.70	15.08
Northern tropics (0°–30°N)	36.13	33.92	17.24	16.21
Southern tropics (0°–30°S)	33.01	31.28	16.45	16.12

lower LST over the polar regions, and cooler LST in nighttime than daytime associated with surface insolation due to the solar zenith angle, are similar in both versions. Larger differences in daytime and nighttime LST can be seen over the arid regions of Africa and Australia. However, a notable difference in magnitude between V6 and V5 can be seen, primarily over the arid regions. V5 shows 2°–4°C less LST than V6 during the daytime over Saudi Arabia, Africa, and South America. However, such underestimation of LST by V5 is mainly concentrated over the desert areas (Sahara Desert, Arabian Desert, and Gobi Desert) in the descending overpasses. Arid regions are the places where LSE uncertainty is high, and hence accurate LST is crucial over these regions (Norouzi et al. 2012). A 3-K difference in LST could lead to about a 1% error in LSE estimates, which is about the level of accuracy that is needed in numerical weather prediction models (Karbou et al. 2005). Moreover, a noticeable overestimation of nighttime LST by V5 when compared with V6 can be observed over the eastern part of the southern polar regions. The underestimation of LST in V5 over the arid regions was found to be more than 2 K when compared with ground-based observations. By refining the retrieval algorithm for V6, Wan (2014) achieved considerably improved LST values. These differences in LST may produce some significant differences in LSE estimates where the new LST product is utilized.

Table 1 shows the mean daytime and nighttime LST averaged for the globe (90°S–90°N), Northern Hemisphere (0°–90°N), Southern Hemisphere (0°–90°S), tropics (30°S–30°N), northern tropics (0°–30°N), and southern tropics (0°–30°S) from both versions of the LST product. The global mean daytime (nighttime) LST from V6 shows 1°C (0.2°C) more than that from V5, whereas it is about 2°C (0.6°C) more in V6 than V5 over the tropics. Figure 2 presents time series of the mean differences in LST between both versions averaged over the globe and over the Northern and Southern Hemispheres for the 13-yr period. A clear seasonal cycle of LST differences can be observed. The underestimation of LST by V5 when compared with V6 is largest during the summer and smallest during the winter season. This seasonal cycle of LST differences is primarily due to the shift in the solar zenith angle. The underestimation of LST by V5 when compared with V6 is larger during daytime than nighttime.

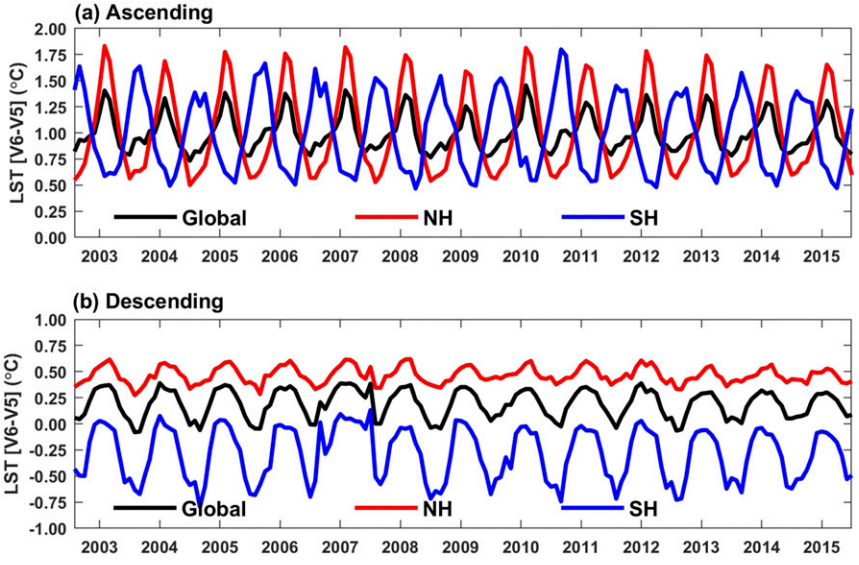

FIG. 2. Time series of interannual mean LST difference (°C) between MODIS *Aqua* V6 and V5 products for day (ascending) and night (descending) overpasses averaged over the globe and Northern and Southern Hemispheres for the period from January 2003 to December 2015.

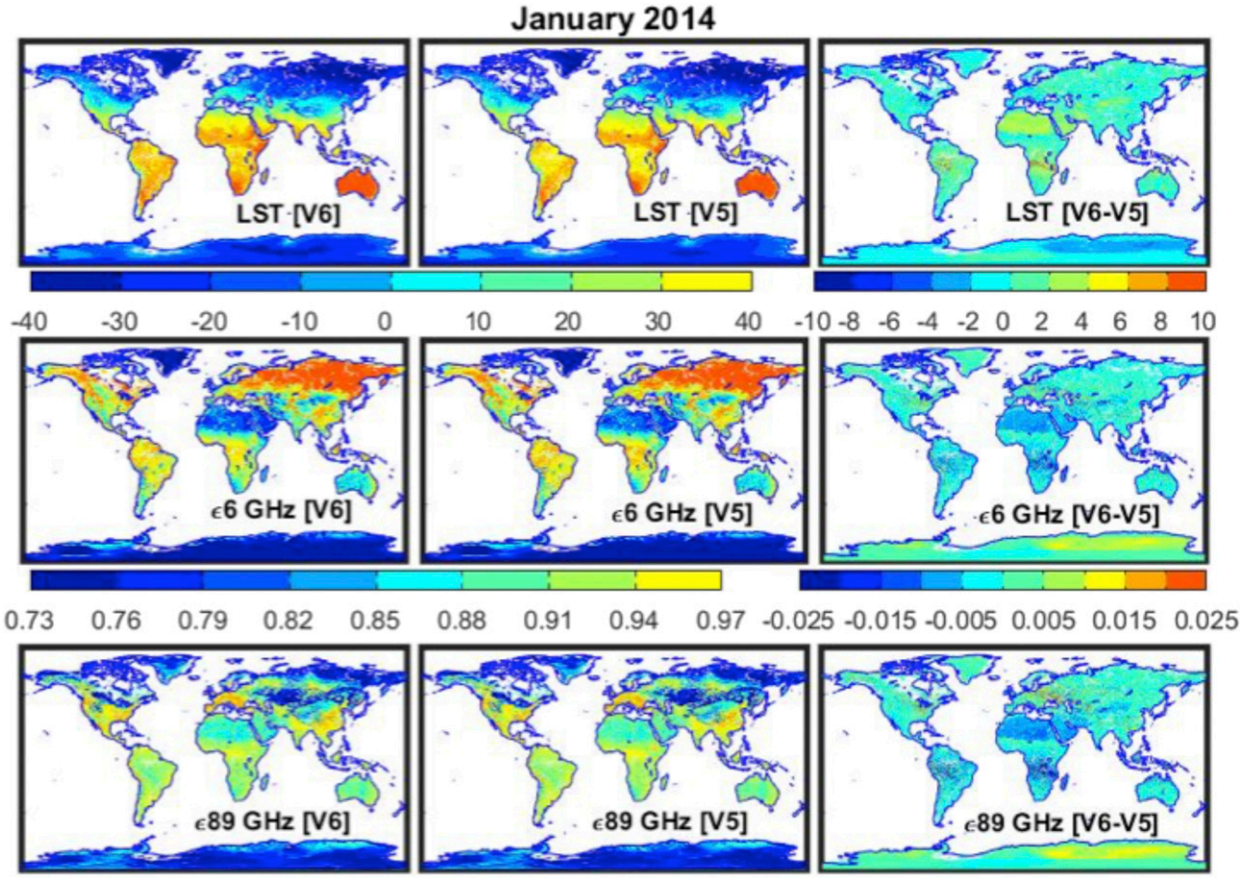

FIG. 3. Mean monthly global LSTs (°C) from MODIS *Aqua* V6 and V5 products and their differences for January 2014. The corresponding AMSR2 global LSEs at 6.925 and 89 GHz, and their differences based on the MODIS-derived LST of V5 and V6 are also shown for horizontal polarization.

b. LSE estimates from AMSR-E and AMSR2 sensors

LST is one of the most important input parameters for the retrieval of LSE. Since MODIS V6 LST shows a noticeable difference from its predecessor V5 (primarily over arid regions), it appears reasonable to characterize the impact of changes in LST product versions over LSE estimates. Figure 3 shows the mean monthly global LST from MODIS V6 and V5 products and their difference for the month of January 2014. The corresponding AMSR2-derived LSE at 6.925 and 89 GHz for horizontal polarization are also shown. Although the spatial patterns of LSE estimates are essentially similar with the use of both versions of the LST product, a considerable LSE difference up to 0.015 in magnitude is observed at both frequency channels over the arid regions associated with the changes in the corresponding LST estimates. Similarly, a notable difference in LST and LSE estimates can be seen over the southern polar regions. In a sensitivity analysis, Norouzi et al. (2011) reported that a 5-K difference in LST would result in an LSE retrieval difference of about 0.025, which is in good agreement with the present analysis. It is also to be noted that similar results were found for other periods; however, only one case study for January 2014 is presented here for brevity. Hence, the MODIS V6 LST product is used to estimate LSE throughout this study.

Because of the deeper penetration of lower-frequency PMW electromagnetic signals over the arid regions with negligible soil moisture content, significant errors are generated in LSE retrievals associated with diurnal variations of LST and Tbs (Prigent et al. 1999; Norouzi et al. 2012, 2015b). A statistical method was recently developed to alleviate the discrepancy between passive microwave Tbs and infrared-based LSTs for diurnal cycles. This statistical method was successfully applied to AMSR2 observations, and it produced more reliable LSE estimates (Prakash et al. 2016). The probability distribution functions (PDFs) of LSE differences between ascending and descending orbits of AMSR-E and AMSR2 over the arid regions for January 2008 and January 2014, respectively, are shown in Fig. 4 for

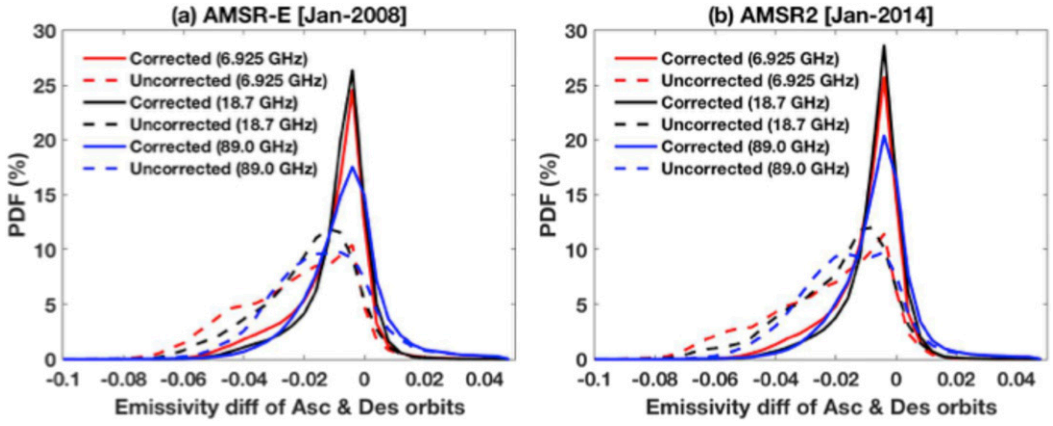

FIG. 4. PDFs of differences in LSE between ascending and descending orbits of AMSR-E and AMSR2 observations before and after applying the correction factor over the global arid regions.

6.925, 18.7, and 89 GHz. The uncorrected LSE differences show a wide range of PDFs, demonstrating an unanticipated difference in LSE from day to night. As expected, the PDF peaks of the corrected LSE are near zero for both sensors because of a negligible diurnal change in moisture. However, the peak is steeper for lower-frequency channels than for higher-frequency channels. This is associated with their relative penetration depths.

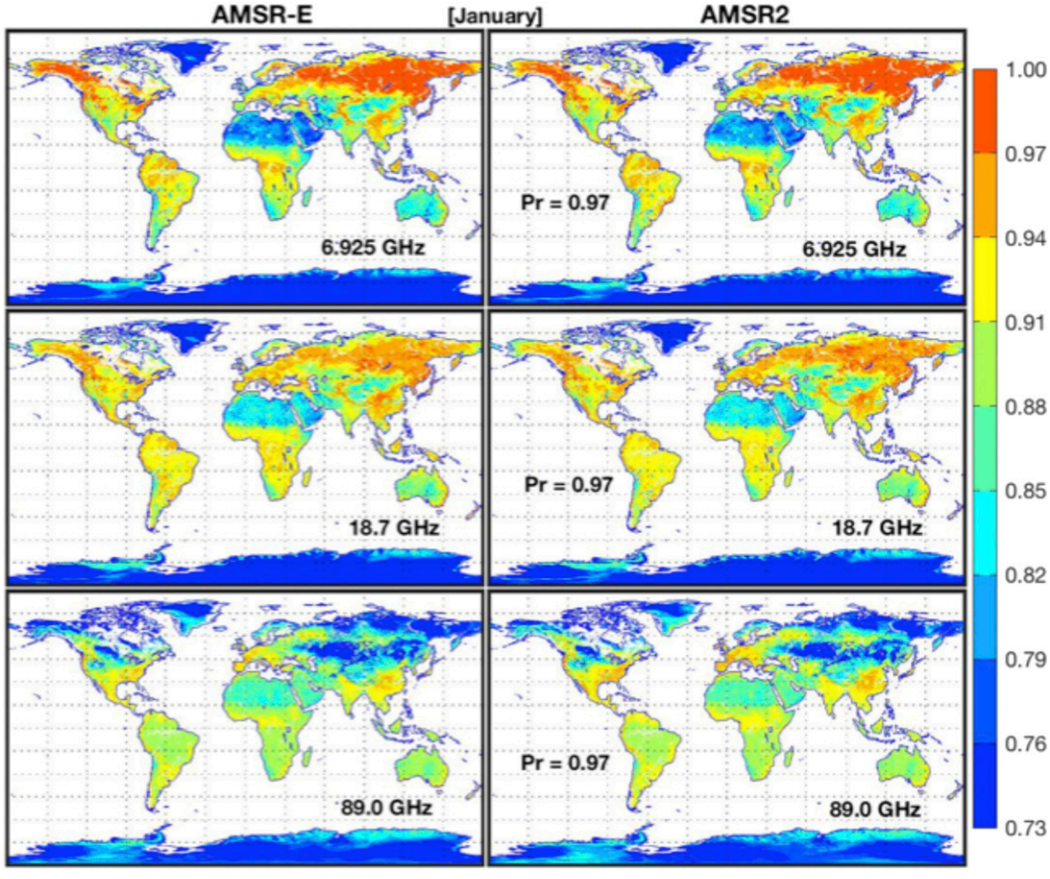

FIG. 5. Mean composite LSE estimates for the month of January from AMSR-E (2003–11) and AMSR2 (2013–17) observations at horizontal polarization for the 6.925-, 18.7-, and 89-GHz channels. The spatial pattern correlations (Pr) between both estimates are also depicted for each channel.

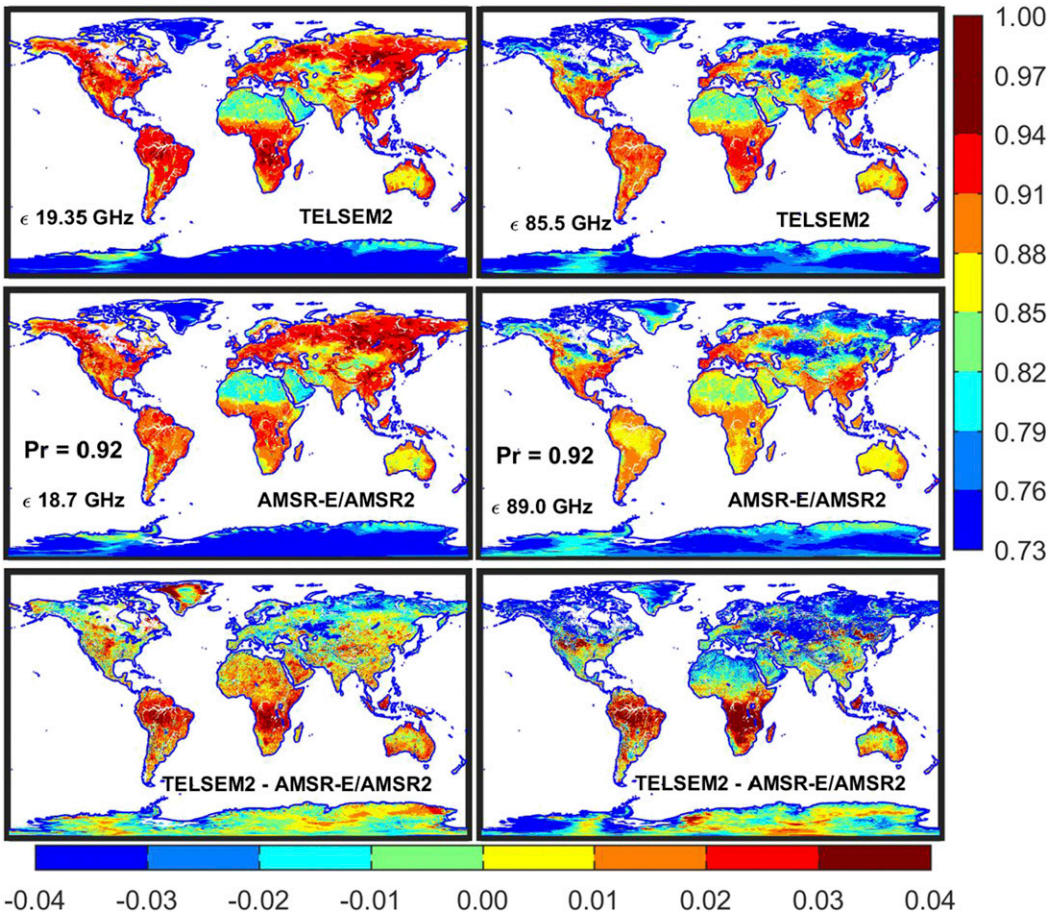

FIG. 6. Spatial distributions of LSE climatology at horizontal polarization from TELSEM^2 and the combined 14-yr AMSR-E/AMSR2 estimates along with their differences for the month of January. The Pr between both estimates are also given.

Hence, the use of a correction factor with infrared-based LST over the arid regions (to obtain an effective temperature) essentially improves the LSE estimates.

Figure 5 shows the intercomparison of mean LSE estimates for the month of January from 9-yr AMSR-E (2003–11) and 5-yr AMSR2 (2013–17) observations. The broadscale LSE features are very well depicted by both estimates. Smaller magnitudes of LSE (e.g., <0.85) over the arid regions such as over the Sahara Desert, the Arabian Desert, and the Gobi Desert were identified by both sensors. This occurrence is due to minimal vegetation and negligible moisture over the arid regions. The impact of seasonal snow cover on LSE estimates over the northern high-latitude regions are also clearly seen at lower- (6.925 GHz) and higher- (89 GHz) frequency channels. Lower-frequency channels show larger magnitudes of LSE, whereas higher-frequency channels show smaller magnitudes of LSE. This result clearly shows that LSE has potential for the detection of seasonal snow cover and its associated soil freezing and thawing. However, permanent ice-covered areas of Greenland and the South Pole show smaller magnitudes of LSE at all channels. LSE values from both sensors show spatial pattern correlations of 0.97 for all frequency channels between the climatologies of the AMSR-E and AMSR2 estimates for the month of January, which reveal that LSE estimates from both sensors are consistent because of the use of coherent ancillary datasets and algorithms.

Since in situ observations of LSE at the global scale are lacking, the estimated LSE values are compared with other satellite-derived estimates. Figure 6 shows the comparison of climatologies of LSE from 14 years of AMSR-E and AMSR2 observations with independent TELSEM^2 land emissivity for the month of January. As TELSEM^2 is derived from the SSM/I observations, the operating frequencies are different from AMSR-E and AMSR2. LSE estimates from two nearby frequency channels (one lower frequency and another higher frequency), and their differences are shown for comparison. Both climatologies of LSE are in reasonably good

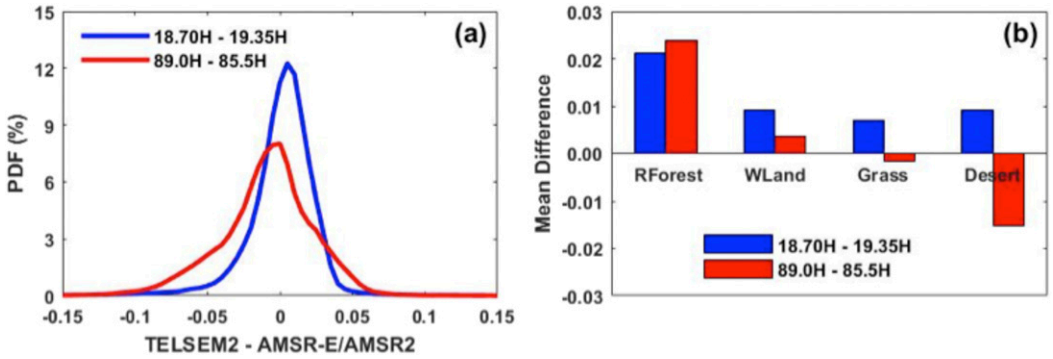

FIG. 7. (a) Differences in the PDFs of mean LSE climatologies from TELSEM^2 and the combined AMSR-E/AMSR2 estimates at horizontal polarization for the month of January and (b) the corresponding mean difference for four distinct land-cover types, viz., evergreen rain forest, deciduous woodland, grassland, and desert regions.

agreement with each other and show spatial pattern correlations of 0.92 at both frequency channels for the month of January, which suggest that about 15% of the variance is explained by other factors. It should also be noted that there are considerable differences in input datasets and sensor characteristics like incidence angle, frequencies, observation time, and ancillary data between SSM/I and AMSR-E/AMSR2 estimates. Moreover, TELSEM^2 shows higher magnitudes of LSE than do the present estimates in the tropics. At higher latitudes of the Northern Hemisphere, TELSEM^2 has lower magnitudes of LSE than AMSR-E/AMSR2 estimates at higher-frequency channels. Figure 7a shows the PDFs of LSE differences between TELSEM^2 and the combined AMSR-E and AMSR2 estimates for the month of January. Both LSE estimates are in good agreement at lower-frequency channels, but there is a notable difference between these two estimates at higher-frequency channels. This difference might be due to water vapor and/or cloud contaminations primarily around the tropics. AIRS atmospheric information has its own uncertainty that could affect the accuracy of LSE estimates at higher frequencies, however, the use of concurrent water vapor and air temperature observations instead of reanalysis data that are used in TELSEM^2 should benefit the present LSE retrieval. The corresponding mean differences in LSE between these two estimates for four different land-cover types are presented in Fig. 7b. The overestimation of LSE by the present estimates when compared with TELSEM^2 linearly decreases with a decrease in vegetation coverage and notably underestimates LSE over the desert regions during January. The LSE measurements from the aircraft campaigns and ground observations primarily over the arid regions are essential to validate satellite-based estimates for further refinements.

Figure 8 shows the PDFs of LSE estimates at horizontal and vertical polarizations of the AMSR-E and AMSR2 sensors for the arid regions. Both sensors exhibit similar characteristics, suggesting the LSE

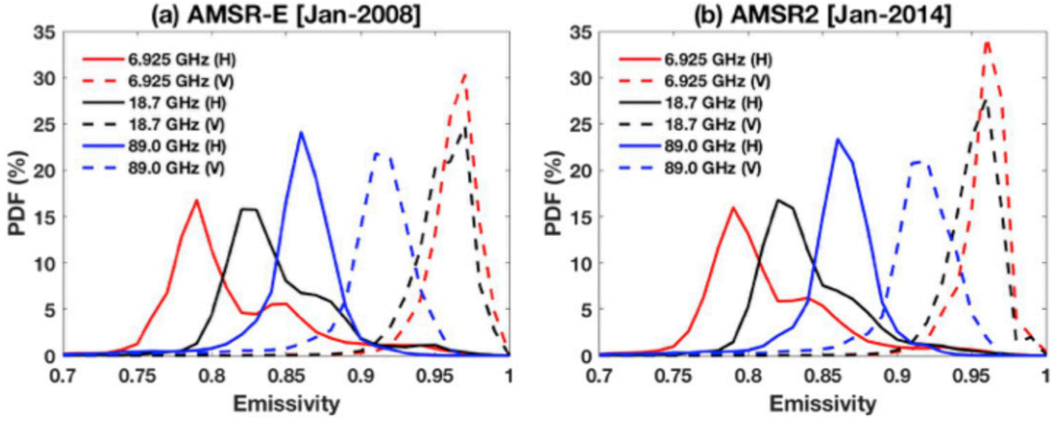

FIG. 8. PDFs of LSE from AMSR-E and AMSR2 observations for vertical and horizontal polarizations averaged over the global arid regions.

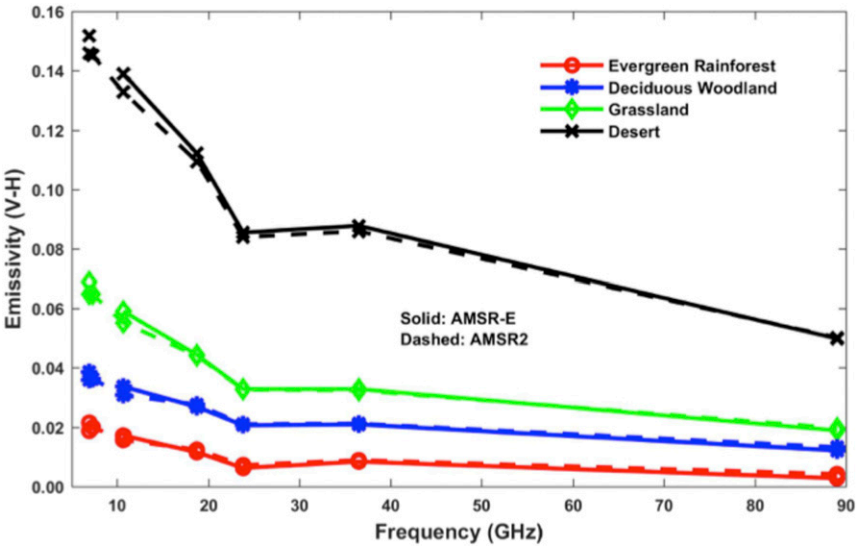

FIG. 9. Variations in mean emissivity differences between vertical and horizontal polarizations for four land-cover types as a function of operating frequencies of the AMSR-E and AMSR2 sensors.

estimates are consistent. In general, LSE shows larger variability associated with larger PDFs at vertical polarization than at horizontal polarization. The differences are largest for the lower-frequency channels, and vice versa. These results are consistent with those from earlier studies by Prigent et al. (1999). Figure 9 presents the variations in mean LSE difference between vertical and horizontal polarizations for four land-cover types as a function of operating frequencies of the AMSR-E and AMSR2 sensors. Both sensors show the same kind of variations in LSE differences with frequency channels. The differences are smallest for the evergreen rain forest and largest for the desert regions. The LSE difference between vertical and horizontal polarizations overall decreases with the increase in frequency for all four land-cover types because of changes in

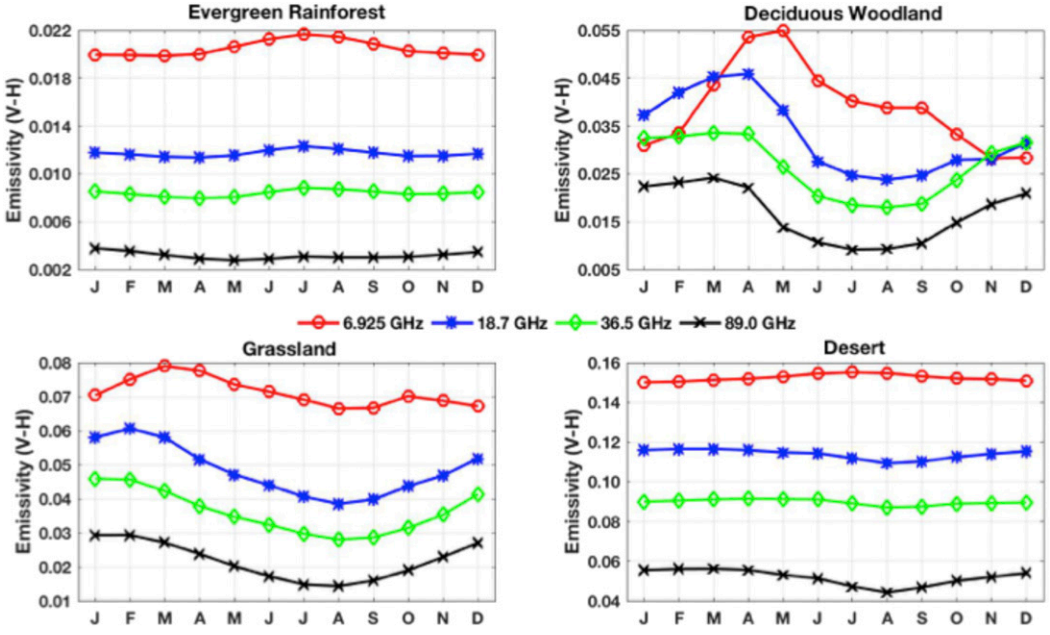

FIG. 10. Monthly variations of emissivity polarization differences ($V - H$) at different frequency channels of AMSR-E/AMSR2 for four land-cover types of the Northern Hemisphere.

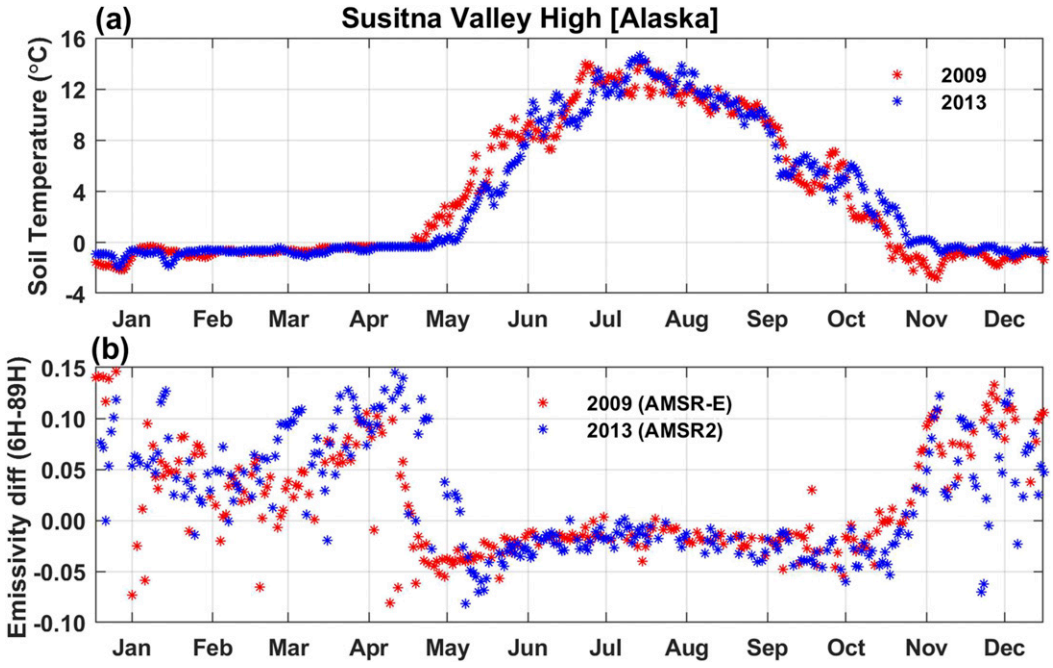

FIG. 11. Time series of daily nighttime (a) 5-cm soil temperature from ground observations and (b) satellite-derived emissivity differences between 6.925 and 89 GHz at horizontal polarization for 2009 and 2013 over a SNOTEL site in Alaska.

penetration depths (Norouzi et al. 2015a). The monthly variations of LSE polarization differences for the four land-cover types in the Northern Hemisphere are presented in Fig. 10 after combining AMSR-E and AMSR2 estimates. As expected, evergreen rain forest and desert regions show negligible seasonal variations in LSE associated with an almost homogeneous surface roughness, whereas deciduous woodland and grassland show considerable seasonal variations of LSE at all frequency channels. The seasonal changes in LSE are associated with the change in biomass density, which is at a minimum during the Northern Hemisphere summer for deciduous woodland and grassland areas.

Because of the sensitivity of LSE with seasonal snow cover, LSE estimates were successfully utilized for high-latitude snowpack detection (Shahroudi and Rossow 2014) and also for soil freeze–thaw state detection (Prakash et al. 2017; Shati et al. 2018). These studies demonstrated that the LSE differences between lower- and higher-frequency channels are good indicators for such analyses. Figure 11 shows the time series of daily nighttime upper-layer soil temperature (e.g., at 5-cm depth) from ground-based observations and the corresponding LSE difference between 6.925 and 89 GHz at horizontal polarization for a specific location in Alaska. Two years, 2009 and 2013, were selected from AMSR-E and AMSR2 spans. The figure shows that colder soil temperature during the Northern Hemisphere winter corresponds to larger differences in LSE estimates, and warmer soil temperature during the Northern Hemisphere summer corresponds to smaller differences in LSE. The range of LSE variations is smaller for the warmer soil than for the colder soil. Hence, the present consistent longer period LSE estimates would essentially be useful for global freeze–thaw and snowpack detection and for other land surface applications.

4. Conclusions

In this study, global cloud-free instantaneous LSEs were estimated for the period from October 2002 to September 2011 from the AMSR-E sensor and for the period from July 2012 to June 2017 from the AMSR2 sensor by using an updated algorithm that alleviated the discrepancy between microwave and infrared observations due to differences in penetration depths. Simultaneous ancillary datasets from the MODIS and AIRS sensors were used for the computation of LSEs; this approach essentially reduced the error of the estimates. The impact of changes in LST on LSE estimates was also assessed by the use of two consecutive versions (V6 and V5) of the LST product that showed noticeable differences over the arid regions. Hence, a careful review of previous findings and products that were based on

earlier version of MODIS LST seems to be necessary. The consistency of LSE estimated by both sensors was examined for different land-cover types. The comparison of global mean LSE features from the combined use of AMSR-E and AMSR2 with an independent product—TELSEM^2—showed spatial pattern correlations on the order of 0.92 at all the frequencies for the month of January. The seasonal variations of the estimated LSE were also investigated for distinct land-cover types. These consistent LSE estimates for a 14-yr period are promising and potentially beneficial for global freeze–thaw and snowpack detection and for other land surface applications. Additionally, the synergism of other available PMW sensors may provide comprehensive global multisatellite LSE estimates to better understand its spatiotemporal variability and underlying processes. Furthermore, extensive efforts are needed for the computation of LSE under all weather conditions by taking into account the effect of clouds in the radiative transfer model and also to comprehensively quantify the uncertainty of LSE estimates.

Acknowledgments. This study is supported by the National Oceanic and Atmospheric Administration Cooperative Science Center for Earth System Sciences and Remote Sensing Technologies (NOAA-CESSRST) under the Cooperative Agreement Grant NA16SEC4810008, by the Department of Defense Army Research Office under Grant W911NF-15-1-0070, by NASA under Grant NNH15ZDA001N, and by the Center for Remote Sensing and Earth System Sciences at the New York City College of Technology. The authors thank the editor and anonymous reviewers for their constructive comments. AMSR-E and AMSR2 brightness temperature data obtained from JAXA (https://gcom-w1.jaxa.jp/), MODIS *Aqua* land surface temperature data obtained from the NASA EOSDID LP DAAC (https://lpdaac.usgs.gov/), and *Aqua*-AIRS data products obtained from the GES DISC (https://disc.gsfc.nasa.gov/) are thankfully acknowledged. The statements contained within the manuscript are not the opinions of the funding agencies or the U.S. government, but reflect the authors' opinions.

REFERENCES

Aires, F., C. Prigent, F. Bernardo, C. Jimenez, R. Saunders, and P. Brunel, 2011: A Tool to Estimate Land-Surface Emissivities at Microwave frequencies (TELSEM) for use in numerical weather prediction. *Quart. J. Roy. Meteor. Soc.*, **137**, 690–699, https://doi.org/10.1002/qj.803.

Birman, C., F. Karbou, and J.-F. Mahfouf, 2015: Daily rainfall detection and estimation over land using microwave surface emissivities. *J. Appl. Meteor. Climatol.*, **54**, 880–895, https://doi.org/10.1175/JAMC-D-14-0192.1.

Didari, S., H. Norouzi, S. Zand-Parsa, and R. Khanbilvardi, 2017: Estimation of daily minimum land surface air temperature using MODIS data in southern Iran. *Theor. Appl. Climatol.*, **130**, 1149–1161, https://doi.org/10.1007/s00704-016-1945-0.

Ferraro, R. R., and Coauthors, 2013: An evaluation of microwave land surface emissivities over the continental United States to benefit GPM-era precipitation algorithms. *IEEE Trans. Geosci. Remote Sens.*, **51**, 378–398, https://doi.org/10.1109/TGRS.2012.2199121.

Gerard, E., F. Karbou, and F. Rabier, 2011: Potential use of surface-sensitive microwave observations over land in numerical weather prediction. *IEEE Trans. Geosci. Remote Sens.*, **49**, 1251–1262, https://doi.org/10.1109/TGRS.2010.2075936.

Karbou, F., C. Prigent, L. Eymard, and J. R. Pardo, 2005: Microwave land emissivity calculations using AMSU measurements. *IEEE Trans. Geosci. Remote Sens.*, **43**, 948–959, https://doi.org/10.1109/TGRS.2004.837503.

Kawanishi, T., and Coauthors, 2003: The Advanced Microwave Scanning Radiometer for the Earth Observing System (AMSR-E), NASDA's contribution to the EOS for global energy and water cycle studies. *IEEE Trans. Geosci. Remote Sens.*, **41**, 184–194, https://doi.org/10.1109/TGRS.2002.808331.

Matzler, C., 2005: On the determination of surface emissivity from satellite observations. *IEEE Geosci. Remote Sens. Lett.*, **2**, 160–163, https://doi.org/10.1109/LGRS.2004.842448.

Noi, P. T., M. Kappas, and J. Degener, 2016: Estimating daily maximum and minimum land air surface temperature using MODIS land surface temperature data and ground truth data in northern Vietnam. *Remote Sens.*, **8**, 1002, https://doi.org/10.3390/rs8121002.

Norouzi, H., M. Temimi, W. B. Rossow, C. Pearl, M. Azarderakhsh, and R. Khanbilvardi, 2011: The sensitivity of land emissivity estimates from AMSR-E at C and X bands to surface properties. *Hydrol. Earth Syst. Sci.*, **15**, 3577–3589, https://doi.org/10.5194/hess-15-3577-2011.

——, W. Rossow, M. Temimi, C. Prigent, M. Azarderakhsh, S. Boukabara, and R. Khanbilvardi, 2012: Using microwave brightness temperature diurnal cycle to improve emissivity retrievals over land. *Remote Sens. Environ.*, **123**, 470–482, https://doi.org/10.1016/j.rse.2012.04.015.

——, M. Temimi, C. Prigent, J. Turk, R. Khanbilvardi, Y. Tian, F. A. Furuzawa, and H. Masunaga, 2015a: Assessment of the consistency among global microwave land surface emissivity products. *Atmos. Meas. Tech.*, **8**, 1197–1205, https://doi.org/10.5194/amt-8-1197-2015.

——, ——, A. AghaKouchak, M. Azarderakhsh, R. Khanbilvardi, G. Shields, and K. Tesfagiorgis, 2015b: Inferring land surface parameters from the diurnal variability of microwave and infrared temperatures. *Phys. Chem. Earth*, **83–84**, 28–35, https://doi.org/10.1016/j.pce.2015.01.007.

Okuyama, A., and K. Imaoka, 2015: Intercalibration of Advanced Microwave Scanning Radiometer-2 (AMSR2) brightness temperature. *IEEE Trans. Geosci. Remote Sens.*, **53**, 4568–4577, https://doi.org/10.1109/TGRS.2015.2402204.

Prakash, S., H. Norouzi, M. Azarderakhsh, R. Blake, and K. Tesfagiorgis, 2016: Global land surface emissivity estimation from AMSR2 observations. *IEEE Geosci. Remote Sens. Lett.*, **13**, 1270–1274, https://doi.org/10.1109/LGRS.2016.2581140.

——, ——, ——, ——, and R. Khanbilvardi, 2017: Potential of satellite-based land emissivity estimates for the detection of

high-latitude freeze and thaw states. *Geophys. Res. Lett.*, **44**, 2336–2342, https://doi.org/10.1002/2017GL072560.

Prigent, C., W. B. Rossow, and E. Matthews, 1998: Global maps of microwave land emissivities: Potential for land surface characterization. *Radio Sci.*, **33**, 745–751, https://doi.org/10.1029/97RS02460.

——, ——, ——, and B. Marticorena, 1999: Microwave radiometric signatures of different surface types in deserts. *J. Geophys. Res.*, **104**, 12 147–12 158, https://doi.org/10.1029/1999JD900153.

——, F. Aires, and W. B. Rossow, 2006: Land surface microwave emissivities over the globe for a decade. *Bull. Amer. Meteor. Soc.*, **87**, 1573–1584, https://doi.org/10.1175/BAMS-87-11-1573.

——, P. Liang, Y. Tian, F. Aires, J.-L. Moncet, and S. A. Boukabara, 2015: Evaluation of modeled microwave land surface emissivities with satellite-based estimates. *J. Geophys. Res. Atmos.*, **120**, 2706–2718, https://doi.org/10.1002/2014JD021817.

Raju, C. S., T. Antony, N. Mathew, K. N. Uma, and K. K. Moorthy, 2013: MT-MADRAS brightness temperature analysis for terrain characterization and land surface microwave emissivity estimation. *Curr. Sci.*, **104**, 1643–1649.

Ringerud, S., C. D. Kummerow, and C. D. Peters-Lidard, 2015: A semi-empirical model for computing land surface emissivity in the microwave region. *IEEE Trans. Geosci. Remote Sens.*, **53**, 1935–1946, https://doi.org/10.1109/TGRS.2014.2351232.

Shahroudi, N., and W. Rossow, 2014: Using land surface microwave emissivities to isolate the signature of snow on different surface types. *Remote Sens. Environ.*, **152**, 638–653, https://doi.org/10.1016/j.rse.2014.07.008.

Shati, F., S. Prakash, H. Norouzi, and R. Blake, 2018: Assessment of differences between near-surface air and soil temperatures for reliable detection of high-latitude freeze and thaw states. *Cold Reg. Sci. Technol.*, **145**, 86–92, https://doi.org/10.1016/j.coldregions.2017.10.007.

Susskind, J., J. M. Blaisdell, and L. Iredell, 2014: Improved methodology for surface and atmospheric soundings, error estimates, and quality control procedures: The Atmospheric Infrared Sounder Science Team version-6 retrieval algorithm. *J. Appl. Remote Sens.*, **8**, 084994, https://doi.org/10.1117/1.JRS.8.084994.

Tian, Y., and Coauthors, 2014: Quantifying uncertainties in land-surface microwave emissivity retrievals. *IEEE Trans. Geosci. Remote Sens.*, **52**, 829–840, https://doi.org/10.1109/TGRS.2013.2244214.

——, C. D. Peters-Lidard, K. W. Harrison, Y. You, S. Ringerud, S. Kumar, and F. J. Turk, 2015: An examination of methods for estimating land surface microwave emissivity. *J. Geophys. Res. Atmos.*, **120**, 11 114–11 128, https://doi.org/10.1002/2015JD023582.

Turk, F. J., L. Li, and Z. Haddad, 2014: A physically based soil moisture and microwave emissivity data set for Global Precipitation Measurement (GPM) applications. *IEEE Trans. Geosci. Remote Sens.*, **52**, 7637–7650, https://doi.org/10.1109/TGRS.2014.2315809.

Wan, Z., 2014: New refinements and validation of the collection-6 MODIS land-surface temperature/emissivity product. *Remote Sens. Environ.*, **140**, 36–45, https://doi.org/10.1016/j.rse.2013.08.027.

Wang, D., and Coauthors, 2017: Surface emissivity at microwaves to millimeter waves over polar regions: Parameterization and evaluation with aircraft experiments. *J. Atmos. Oceanic Technol.*, **34**, 1039–1059, https://doi.org/10.1175/JTECH-D-16-0188.1.